

Quantum meets classical phase transition: Low-temperature anomaly in disordered superconductors near B_{c2}

Benjamin Sacépé,¹ Johanna Seidemann,¹ Frédéric Gay,¹ Kevin Davenport,²
Andrey Rogachev,² Maoz Ovadia,³ Karen Michaeli,³ and Mikhail V. Feigel'man^{4,5}

¹*Univ. Grenoble Alpes, CNRS, Grenoble INP, Institut Néel, 38000 Grenoble, France*

²*Department of Physics and Astronomy, University of Utah, Salt Lake City, Utah 84112, USA*

³*Department of Condensed Matter Physics, The Weizmann Institute of Science, Rehovot 76100, Israel.*

⁴*L. D. Landau Institute for Theoretical Physics, Chernogolovka, 142432, Moscow region, Russia*

⁵*Skolkovo Institute of Science and Technology, Moscow 143026, Russia*

Strongly disordered superconductors in a magnetic field display many characteristic properties of type-II superconductivity— except at low temperatures where an anomalous linear T -dependence of the resistive critical field B_{c2} is routinely observed. This behavior violates the conventional theory of superconductivity, and its origin remains a long-standing puzzle. Here we report on systematic measurements of the critical magnetic field and current on amorphous indium oxide films of various levels of disorder. Surprisingly, our measurements show that the B_{c2} anomaly near zero-temperature is accompanied by a clear mean-field like scaling behavior of the critical current. We demonstrate theoretically that these are consequences of the vortex-glass ground state and its thermal fluctuations. This theory further predicts the linear- T anomaly to occur in films as well as bulk superconductors with a slope that depends on the normal-state sheet resistance—in agreement with experimental data. Thus, our combined experimental and theoretical study reveals universal low-temperature behavior of B_{c2} in a large class of disordered superconductors.

The magnetic-field tuned transition of disordered superconductors continues to surprise as well as to pose intriguing and challenging puzzles. A wealth of experimental results obtained over decades of study still defies current theoretical understanding. The anomalous temperature dependence of the resistive critical field $B_{c2}(T)$ near the quantum critical point between superconductor and normal metal is a well known example. Within the conventional Bardeen-Cooper-Schrieffer theory, $B_{c2}(T)$ is expected to saturate at low temperatures^{2,12}. In contrast, a strong upturn of B_{c2} with a *linear- T* dependence as $T \rightarrow 0$ has been observed in numerous disordered superconductors. These systems range from alloys and oxides, both in thin films^{3–9} and bulk¹⁰, to boron-doped diamond¹¹ as well as gallium monolayers¹².

Substantial theoretical efforts^{13–17} have been unable to fully resolve the origin of this anomalous behavior. The main challenge lies in the complexity of these systems and the subtle interplay between strong fluctuations, disorder and vortex physics. The prevailing explanation for the low- T anomaly of $B_{c2}(T)$ is based on mesoscopic fluctuations^{13,14}, which result in a spatially inhomogeneous superconducting order parameter. A recent alternative interpretation invokes a quantum Griffiths singularity to account for the upturn in $B_{c2}(T)$ observed in ultra-thin gallium films¹². While these theoretical approaches are generally plausible, they predict an exponential increase of $B_{c2}(T)$ at very low T , which manifestly does not capture the specific *linear* dependence measured in disordered superconductors^{3–12}.

To gain new insights on the underlying physical mechanism it is desirable to not only study $B_{c2}(T)$, but to also extract information on additional characteristic quanti-

ties such as the superfluid stiffness. We therefore conducted systematic measurements of both B_{c2} and the critical current j_c in films of amorphous indium oxide (a:InO), a prototypical disordered superconductor. In the absence of magnetic field or when vortices are strongly pinned by disorder (i.e., form a vortex glass) the superfluid stiffness can be directly related to the critical current. This is expected to apply to all materials that exhibit the low-temperature B_{c2} anomaly^{3–12}. Consequently, measurements of $j_c(B)$ near zero temperature provide access to the critical behavior of the superfluid density $\rho_s(B)$ near $B_{c2}(0)$, where the low- T anomaly develops.

The key experimental finding of this work is that the (well-established) linear T -dependence of $B_{c2}(T)$ at low temperatures is accompanied by a *power-law* dependence of the critical current on B . The critical exponent of $j_c(B) \sim |B - B_{c2}|^v$ is found to be $v \simeq 1.6$. As explained below, this is consistent with the mean field value $v = 3/2$ (but not with the mesoscopic fluctuation scenario^{13,14} which predicts an exponential dependence¹⁴). Our unexpected finding has direct implication for the critical behavior of $\rho_s(B)$, and demands a revised theory of disordered superconductors in the presence of magnetic field. We therefore complement our experimental work with a comprehensive theoretical study, which identifies the key to understanding the linear T -dependence of B_{c2} in the vortex glass. When vortices are strongly pinned by impurities, their presence only weakly affects the $T = 0$ limit of superfluid stiffness and critical current. As a result, both exhibit mean-field-like dependence on the magnetic field. In contrast, the temperature variation of the superfluid stiffness is strongly affected by thermal fluctua-

tions of the vortex glass. This gives rise to the observed linear T -dependence of $B_{c2}(T)$ near the quantum critical point. Moreover, we predict a strong dependence of the slope $dB_{c2}(T)/dT|_{T \rightarrow 0}$ on the sheet resistance, and consequently on the film thickness, which we confirm experimentally.

Low- T anomaly near $B_{c2}(0)$

In this study we focus on a series of a:InO samples, which exhibit a critical temperature between $T_c = 3$ K and 3.5 K and a sheet resistance before transition between $2k\Omega$ and $1.2k\Omega$ (see Table S1 in SI). Those samples are far from the disorder-tuned superconductor-insulator transition and behave in many ways as standard dirty superconductors. Their magneto-transport properties upon varying disorder are presented in our previous work⁹. Moreover, to demonstrate the universal role of disorder in the low- T anomaly of $B_{c2}(T)$, we extended our measurements to another thin film material, amorphous molybdenum-germanium¹ (MoGe); the characterizing parameters as well as the experimental data are presented in the SI.

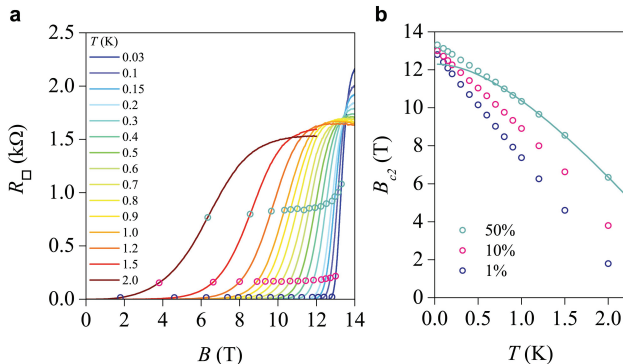


FIG. 1: **Low- T anomaly of the upper critical field $B_{c2}(T)$.** **a**, R_{\square} versus B measured at fixed temperatures for sample J033. Open circles indicate the determination of $B_{c2}(T)$ using three different criteria, namely 50, 10 and 1% of the high field normal state resistance. **b**, Extracted $B_{c2}(T)$ values from the measurement shown in **a**, plotted versus T . The solid line is a high temperature fit using the theory for dirty superconductors^{2,12}.

Figure 1a displays the magneto-resistance isotherms of sample J033 measured down to 0.03 K. We define the critical magnetic field B_{c2} through the resistive transition, i.e., the onset of superconducting phase coherence. This critical field does not coincide with the one associated with the pairing instability (see also the discussion in Section IV). To determine B_{c2} at each temperature we used three different criteria, namely 1, 10 and 50% of the normal state resistance at high field, indicated by open dots on magneto-resistance isotherms. The resulting B_{c2} versus T curves are shown in Fig. 1b together with a fit (solid-line) of the high-temperature data with the theory for dirty superconductors^{2,12}. We see that $B_{c2}(T)$ deviates below $\lesssim 1$ K from the fit and increases linearly with

decreasing T down to our base temperature of 0.03 K (see SI). This deviation, which is the focus of this work, is independent of the criterion used to determine B_{c2} .

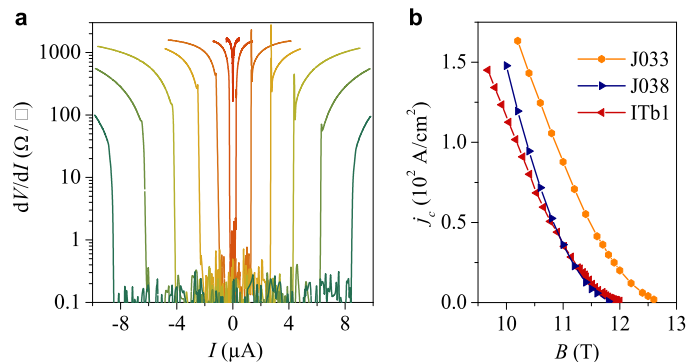


FIG. 2: **Critical current density j_c near $T = 0$ and $B_{c2}(0)$.** **a**, dV/dI versus I of sample J033 measured at $T = 0.03$ K and at magnetic fields of 10.4, 10.8, 11.2, 11.6, 12, 12.5 and 13 T (green to red curves respectively). **b**, j_c versus B of both samples J033, ITb1 and J038. Each values of $j_c(B)$ were extracted from dV/dI versus I measurements as shown in **a** at the resistance value of $dV/dI = 10\Omega/\square$.

An important aspect of the linear dependence of $B_{c2}(T)$ is that it persists down to our lowest T approaching the quantum phase transition QPT at $B_{c2}(0)$. We shall argue below that the linear dependence of $B_{c2}(T)$ can be understood by analyzing the critical behavior of the superfluid density in the vicinity of this QPT.

Critical regime of the critical current density

We turn to the study of the B -evolution of the critical current density j_c at our lowest temperature and focus on three samples J033, ITb1 and J038. We systematically measured the differential resistance dV/dI versus current-bias I at fixed B 's. As shown in Fig. 2a, on increasing I , a sudden, non-hysteretic jump occurs in the dV/dI curve, indicating the critical current value. The resulting critical current density j_c for both samples is plotted versus B in Fig. 2b. Interestingly, the continuous suppression of j_c with increasing B tails off prior to vanishing at a critical field $B_{c2}^{jc} = 12.8$ T, 12.1 T and 11.9 T for samples J033, ITb1 and J038 respectively. Such a resilience of j_c to the applied B when approaching $B_{c2}(0)$ is reminiscent of the anomalous upturn of the $B_{c2}(T)$ line at low T . We also notice that the critical field values B_{c2}^{jc} at which j_c vanishes slightly differ from $B_{c2}(0)$ obtained in Fig 1 ($B_{c2}(0) = 13.3$ T, 12.4 T and 12.6 T determined with the 50 % criterion for samples J033, ITb1 and J038 respectively). The reasons for this disparity stem from the finite-resistance criterion used to determine $B_{c2}(T)$, which does not coincide with the termination of superconducting current at B_{c2}^{jc} .

The key result of this work is shown in Fig. 3 where j_c is plotted in logarithmic scale as a function of $|B_{c2}^{jc} - B|$. By adjusting the value of B_{c2}^{jc} in the x-axis to 12.8, 12.1 and 11.9 T for samples J033, ITb1 and J038 respectively, one obtains clear straight lines that unveil a scaling rela-

tion of the form:

$$j_c(B) = j_c(0) \left| 1 - \frac{B}{B_c^{j_c}} \right|^\nu, \quad (1)$$

where the fitted values for the exponent ν are 1.62 ± 0.02 , 1.67 ± 0.02 and 1.65 ± 0.02 for samples J033, ITb1 and J038 respectively. The prefactor $j_c(0)$ falls in the range $(2.5-4) \cdot 10^3 \text{ A/cm}^2$ for all three samples. The inset of Fig. 3 shows the sensitivity of the straight line to $B_c^{j_c}$, where a small variation of 0.05T yields a significant deviation from linearity. We furthermore present in the SI similar results obtained on a MoGe sample, which demonstrate the universality of this scaling relation. It is noteworthy that the values of the exponent are within 10% of the mean-field value $3/2$ of the classical temperature-driven superconducting transition in the absence of magnetic-field. Ginzburg-Landau theory predicts that the critical current would be $j_c^{GL} \propto \rho_s / \xi_{GL} \propto (T_c - T)^{3/2}$, with the Ginzburg-Landau superconducting coherence length $\xi_{GL} \propto (T_c - T)^{-1/2}$ and $\rho_s \propto (T_c - T)$. This striking similarity suggests that also the scaling of $B_{c2}(T)$ and $j_c(B)$ low temperature may be captured by mean-field theory of the bulk material.

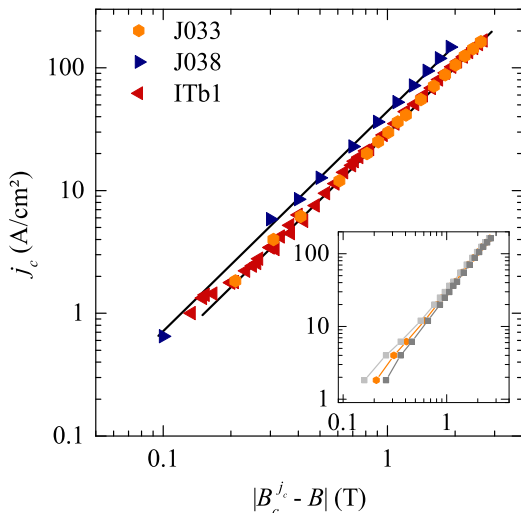


FIG. 3: **Scaling of the critical current density with magnetic field.** j_c versus $|B_c^{j_c} - B|$. The $B_c^{j_c}$ values are adjusted to obtain straight lines that are emphasized by black solid-lines. Inset: the dark grey and light grey curves are the data of sample J033 plotted with $B_c^{j_c} \pm \delta$, where $\delta = 0.05$ T.

Interpretation of experimental results within mean-field theory

The mean-field critical exponent of $j_c(B)$ at $T = 0$ near $B_{c2}(0)$ can be extracted from the Ginzburg-Landau free energy which reads:

$$F = \alpha |\Delta(\mathbf{r})|^2 + \beta |\Delta(\mathbf{r})|^4 + \gamma \left| \left(-i\nabla - \frac{2e}{\hbar c} \mathbf{A}(\mathbf{r}) \right) \Delta(\mathbf{r}) \right|^2. \quad (2)$$

Within mean-field theory, the coefficient α strongly de-

pends on temperature and magnetic field¹⁹:

$$\alpha = \nu \left[\ln \frac{T}{T_{c0}} + \psi \left(\frac{1}{2} + \frac{eDB}{2\pi cT} \right) - \psi \left(\frac{1}{2} \right) \right]. \quad (3)$$

Here, D and ν are the electron diffusion coefficient and density-of-states respectively, and $\psi(x)$ is the digamma function. B in Eq. (3) is the magnetic field penetrating the superconductor. While for type-II superconductors such as our a:InO films this magnetic field can be non-uniform at low B , close to B_{c2} the spatial fluctuations of B are negligible, and the average magnetic field is equal to the externally applied one. The other two parameters of the Ginzburg-Landau functional, β and $\gamma \propto \nu D$ depend only weakly on temperature and magnetic field. Consequently, Eq. (2) captures the two effects of magnetic field on superconductors: The suppression of the transition point due to pair-breaking (through the parameter α), and the diamagnetic response captured by the vector potential \mathbf{A} . Note that the expression for α in Eq. (3) is typical for superconductors in the presence of a pair-breaking mechanism²⁰. For example, the effect of magnetic impurities can be captured by replacing the magnetic field by a term proportional to the spin relaxation rate Γ^{12} . Correspondingly, these systems have the same $T = 0$ critical exponents (i.e. $\alpha \approx |1 - B/B_{c2}|$ or analogously $\alpha \approx |1 - \Gamma/\Gamma_c|$). The mean-field treatment is performed under the assumption that vortices are strongly pinned. As a result, the presence of magnetic field induced vortices can be neglected, and j_c is proportional to the depairing current. A detailed explanation of the origin and the consequences of strong pinning is given in the next section.

The $T = 0$ limit of Eq. (2) yields the magnetic-field dependence of the order parameter and the coherence length near the quantum critical point, $|\Delta(B)| \sim |B - B_{c2}|^{1/2}$ and $\xi_{GL}(B) \approx \xi_0 |1 - B/B_{c2}|^{-1/2}$ (where $\xi_0 \approx 5$ nm in our a:InO samples, see Ref. 9.) The latter, together with the superfluid stiffness ρ_s , determines the mean-field value of the critical de-pairing current: $j_c^{GL} \propto \rho_s / \xi_{GL}$. To find the superfluid stiffness, we match the superconducting current extracted from the free energy, $\mathbf{j} = -c\partial F/\partial \mathbf{A}$, with the London equation, $\mathbf{j} = -4\rho_s e^2 \mathbf{A} / \hbar^2 c$. We find that

$$\rho_s(B) = \frac{12}{\pi} \rho_{s0} \left(1 - \frac{B}{B_{c2}(0)} \right), \quad (4)$$

and the relation between the superfluid stiffness and the critical current yields

$$j_c^{GL}(B) = \frac{8e}{3\sqrt{3}\pi\hbar\rho_s(B)\xi_{GL}(B)} = j_c^{GL}(0) \left(1 - \frac{B}{B_{c2}} \right)^{3/2}. \quad (5)$$

The corresponding critical exponent $\nu = 3/2$ is in excellent agreement with our experimental findings. The prefactor $j_c^{GL}(0)$ can be estimated using the experimental data of Ref. 14, where the superfluid stiffness of 20 nm

thick a:InO films was measured. From their experimental results at low magnetic field, we estimate the critical current to be $j_c^{GL}(0) \sim 10^4 \text{ A/cm}^2$ —larger than our experimentally observed value only by a factor of ~ 4 . This is a non-trivial observation which is in contrast to a weakly pinned vortex state where the critical current is set by the de-pinning current $j_c^{\text{depin}} \ll j_c^{GL}$. It also provides an important hint to the origin of the anomalous critical magnetic field and, as we show below, follows naturally from our theory.

To complete the comparison between the experimental results and mean-field theory, we extract the low-temperature critical field from the condition $\alpha(B, T) = 0$. We note that within mean field theory the resistive critical magnetic field coincides with the onset of pairing, B_{c2} . We find $B_{c2}(0) - B_{c2}(T) \sim T^2$, which is inconsistent with the linear dependence $B_{c2}(0) - B_{c2}(T) \sim T$ that is observed experimentally (see Fig. 2). Power-laws with exponent smaller than two are known to arise in strongly correlated superconductors^{21–25}. In the context of high T_c cuprates, the deviation from mean-field result has been attributed²³ to an extended region of strong fluctuations around $B_{c2}(T)$. However, in conventional superconductors, such as the a:InO films studied here, the region of strong fluctuations is small and the Ginzburg-Landau theory is expected to describe the onset of pairing at all temperatures and magnetic fields²³. Indeed, mean-field theory captures the scaling of the critical temperature with magnetic field at low B . This indicates that to understand the low temperature behavior of $B_c(T)$ other beyond-mean-field effects should be considered. In particular, Ginzburg-Landau theory does not include thermal fluctuations of the vortex-glass, which are essential in the finite-temperature transition to the normal state. As we will show below, these fluctuations are the key ingredient to understanding the linear- T dependence of B_{c2} ; however, they do not change the scaling behavior of $j_c(B, 0)$.

Vortex-glass fluctuations

In low-dimensional superconductors the pairing instability is known to differ from the onset of phase coherence. A prominent example is the Berezinskii-Kosterlitz-Thouless (BKT) transition in thin films^{26,27}. Similar decoupling is known to occur in moderately-disordered type-II superconductors near B_{c2} , where the magnetic field gives rise to the formation of a weakly pinned vortex lattice^{28,29}. Moreover, the superconducting state becomes resistive when the force applied on the vortex lattice by the current exceeds the pinning forces. The corresponding de-pinning critical current j_c^{depin} is then significantly lower than the pair-breaking critical current extracted from the Ginzburg-Landau theory, j_c^{GL} , and it is not expected to obey simple scaling behavior^{29,30} close to B_{c2} .

In contrast, in highly disordered superconductors such as our a:InO films, we expect a strongly pinned vortex-glass^{29,32} to form. This is caused by large spatial fluctuations of the order parameter³³, which are predicted

by the theory of "fractal" superconductors¹⁵ to arise in disordered systems such as the a:InO films in question. According to this theory,¹⁵ in the absence of a magnetic field, the superconducting condensation energy E_g fluctuates strongly in space, $\delta E_g \sim E_g$, over distances comparable to the coherence length ξ . Correspondingly, core energies of vortices, which are induced by an applied magnetic field, exhibit similar fluctuations, and hence become strongly pinned. In fact, vortices pinning in such systems resembles the one found in models of columnar defects³¹. Upon applying a current, vortices de-pin only when the superconducting order parameter is sufficiently reduced, i.e., within mean-field theory j_c^{depin} scales like the Ginzburg-Landau de-pairing current. Thus, in our system $j_c^{\text{depin}} = \Upsilon j_c^{GL}$ where $\Upsilon < 1$ (for example, in the model of Ref.³¹, $\Upsilon \approx 1/3$), and the I-V curves are expected to follow those studied theoretically in Ref. 42. Consequently, Eq. (5) still applies even in the presence of vortices.

The above analysis implies that the main corrections to the mean-field values of the critical field and current in highly disordered superconductors are due to renormalization of the superfluid stiffness caused by fluctuations of the vortex glass³². To estimate the modified ρ_s , we focus exclusively on phase-fluctuations of the order parameter, i.e. $\Delta(\mathbf{r}) = |\Delta_0|e^{i\Phi(\mathbf{r})}$. Inserting this into the free energy, Eq. (2), yields $F[\Phi] = \rho_s [\nabla\Phi(\mathbf{r}) - \frac{2e}{\hbar c}\mathbf{A}(\mathbf{r})]^2/2$. It is convenient to further separate $\Phi(\mathbf{r})$ into smooth phase fluctuations (the superfluid mode) $\varphi(\mathbf{r})$ with $\nabla \times \nabla\varphi = 0$ and fluctuations of the vortex-glass $\psi(\mathbf{r})$, with $\Phi(\mathbf{r}) = \varphi(\mathbf{r}) + \psi(\mathbf{r})$. We determine the renormalized superfluid stiffness via the static current-current correlation function $\langle J_{sc}^i(\mathbf{r}, \omega_n = 0) \rangle = \int d\mathbf{r} \langle J_{sc}^i(\mathbf{r}, 0) J_{sc}^j(0, 0) \rangle A^j(0, 0)$, where as before $\mathbf{J}_{sc}(\mathbf{r}) = -c\partial F/\partial\mathbf{A}(\mathbf{r})$. Since ρ_s is determined by the long-wavelength properties, it is sufficient to focus on length-scales larger than the (typical) inter-vortex spacing a_0 . Moreover, within such a coarse-grained description, the coupling between superfluid and vortex fluctuations is local.

We note that a charge encircling a vortex acquires phases from both the external and the vortex field, $\oint [\nabla\psi(\mathbf{r}) - 2e/\hbar c\mathbf{A}(\mathbf{r})] \cdot d\boldsymbol{\ell}$. If the vortices were uniformly spaced (a vortex lattice), the two contributions to the phase would cancel at a length scale a_0 . In the coarse grained description and in the symmetric gauge for the vector potential, this amounts to $\nabla\psi(\mathbf{r}) = \mathbf{A}(\mathbf{r})$. In a vortex-glass this cancellation is not exact. Still, near B_{c2} and at the length scales of $a_0 = \sqrt{\Phi_0/B} \approx \xi_0\sqrt{2\pi}$, the density of vortices is nearly uniform. We introduce the field $\mathbf{R}(\mathbf{r}) = (R_x(\mathbf{r}), R_y(\mathbf{r}))$ that describes the deviation of the vortex positions from uniformity. \mathbf{R} thus encodes the particular realization of the vortex-glass, and, in the absence of forces, its spatial average vanishes,

$V^{-1} \int d\mathbf{r} \mathbf{R}(\mathbf{r}) = 0$. It is thus appropriate to expand

$$\begin{aligned} \nabla\psi(\mathbf{r} - \mathbf{R}(\mathbf{r})) - \frac{2e}{\hbar c} \mathbf{A}(\mathbf{r}) &\approx -\frac{2e}{\hbar c} (\mathbf{R}(\mathbf{r}) \cdot \nabla) \mathbf{A} \quad (6) \\ &= \frac{\mathbf{u}(\mathbf{r}) \times \hat{z}}{2a_0}. \end{aligned}$$

where $\mathbf{u}(\mathbf{r}) = 2\pi\mathbf{R}(\mathbf{r})/a_0$ is the dimensionless displacement field. It follows that the leading coupling terms in the free energy between φ and \mathbf{u} are

$$\delta F = \rho_s a_0^{-1} \hat{z} \cdot [\nabla\varphi(\mathbf{r}) \times \mathbf{u}(\mathbf{r})] - C\rho_s (\nabla\varphi(\mathbf{r}))^2 \mathbf{u}^2(\mathbf{r}), \quad (7)$$

where C is a material specific coefficient of order unity. Note that here we assume isotropy in the $x - y$ plane.

The first term in Eq. (7) corresponds to the lowest order expansion with respect to gradients in the Ginzburg-Landau free energy (2). It gives rise to a temperature and magnetic-field independent correction to the superfluid stiffness that depends on the realization of the vortex-glass. This reduction enters the measurable quantity ρ_{s0} which we treat as a phenomenological parameter. As we show below, higher-order gradients (like the second term in Eq. (7)) become important at non-zero temperature. The leading contribution of such terms to ρ_s is given by

$$\delta\rho_s^{x,y} = -\frac{C\rho_s}{a_0^3} T \sum_n \int d\mathbf{r} \langle \mathbf{u}(\mathbf{r}, \omega_n) \cdot \mathbf{u}(0, -\omega_n) \rangle. \quad (8)$$

It remains to evaluate the $\mathbf{u} - \mathbf{u}$ correlation function. In the strong pinning regime, a restoring force acts to keep the vortex structure near its local energy minimum. Consequently, it is sufficient to reduce the equation of motion to its local form for $\mathbf{u}(\mathbf{r}, t)$, which describes individual vortices²⁹, and in addition neglect spatial gradients of the $\mathbf{u}(\mathbf{r})$ field

$$\eta\partial_t \mathbf{u}(\mathbf{r}, t) + \kappa(\mathbf{u}(\mathbf{r}, t) - \mathbf{u}_0(\mathbf{r})) = \mathbf{f}(t) \equiv \frac{\hbar a_0}{2e} \mathbf{j} \times \hat{z}, \quad (9)$$

where $\mathbf{u}_0(\mathbf{r})$ is the static displacement at zero current. The r.h.s. of Eq.(9) is the Lorentz force acting on a segment of a vortex of length a_0 in presence of a supercurrent \mathbf{j} . We emphasize the absence of gradients of \mathbf{u} in the equation of motion—this manifests the locality of the vortex dynamics. Effectively, the vortex fluctuations in the glass state at low temperature resemble a (damped) optical phonon mode. The parameter

$$\eta = (\hbar/2e)^2 \sigma_n / 2\pi = \frac{\pi\hbar^2}{2e^2} \sigma_n$$

reflects the presence of normal electrons in the vortex cores, whose resistance σ_n^{-1} gives friction to the vortex motion (note that we defined friction coefficient η w.r.t. dynamics of dimensionless coordinate $\mathbf{u} = 2\pi\mathbf{R}/a_0$). For strongly disordered materials $\sigma_n a_0 \sim e^2/\hbar$ and thus $\eta \sim \hbar/a_0$. This overdamped character of the vortex mo-

tion leads us to neglect the inertial term $\propto \partial_t^2 \mathbf{u}$ with respect to friction. Likewise, we neglect the contribution to the Lorentz force due to vortex velocity since it does not affect the relevant current-current correlation function. The parameter κ can be determined similar to the penetration length in pinned vortex systems, also known as the Campbell length³⁵⁻³⁷ (for a recent review see Ref.³⁸). According to Eq.(9), the shift of \mathbf{u} due to current \mathbf{j} is equal to $\mathbf{u}(\mathbf{r}) - \mathbf{u}_0(\mathbf{r}) = \hbar a_0 (\mathbf{j} \times \mathbf{n}) / 2e\kappa$. The corresponding shift of the vortex magnetic flux can be expressed through $\delta\mathbf{A} = -\hbar\Phi_0 \mathbf{j} / 4e\kappa a_0$. Using the London relation, we get $\kappa = \pi\rho_s$. From Eq. (9) we obtain the Matsubara Green's function of \mathbf{u}

$$G(\mathbf{r}, \omega_n \neq 0) = a_0^2 \delta(\mathbf{r}) [\eta|\omega_n| + \kappa]^{-1}. \quad (10)$$

We thus arrive at the reduction of the superfluid stiffness due to thermal fluctuations of the vortex-glass. Combining Eqs. (8) and (10) yields the following correction to the superfluid stiffness $\delta\rho_s(T, B) = \rho_s(T, B) - \rho_s(0, B)$:

$$\begin{aligned} \delta\rho_s(T, B) &= - \left[T \sum_n [\eta|\omega_n| + \kappa]^{-1} \right. \\ &\quad \left. - \int \frac{d\omega}{2\pi} [\eta|\omega| + \kappa]^{-1} \right] = -C \frac{\hbar\sigma_n}{e^2} \frac{T^2}{3\pi\rho_s(B)a_0}. \end{aligned} \quad (11)$$

The last equality holds in the low-temperature limit $T/\hbar \ll \kappa/\eta$; in the opposite limit one recovers the classical result $\langle \mathbf{u}^2 \rangle = T/\kappa$. The smallness of the low temperature result $\delta\rho_s(T, B) \propto T^2$ is compensated by the small $\rho_s(B) \propto 1 - B/B_{c2}(0)$ in the denominator, see Eq.(4). This new result is unique for disordered superconductors, in which the fluctuations at $T > 0$ are controlled by the dissipation in the gapless vortex cores, and it provides the key to understanding the low- T linear upturn of B_{c2} .

Thermal fluctuation corrections to the critical current

To substantiate the correction to the superfluid stiffness given in Eq. (11), we conducted additional measurements of the temperature dependence of the critical current in the vicinity of $B_{c2}(0)$. The differential resistance dV/dI as a function of current measured on sample ITb1 at various temperatures and fixed $B = 11.25$ T is shown in Figure 4a. A clear jump in the resistance, similar to that in Fig. 1a, develops at ultra-low temperatures and indicates the position of j_c . At higher temperatures, the critical current decreases and a non-zero resistance is found already before the jump. This resistance at sub-critical current rises above the noise level for $T > 0.05$ K, and exhibits a clear exponential increase with the current, which is highlighted by the black dashed-line in this semi-log plot. Such resistance curves are expected to be observed when the vortex glass is strongly pinned: The resistance at low current is a typical signature of vortex creep, where the Lorentz force induced by the current reduces the barrier. Above j_c , the corresponding current-voltage characteristics show an excess current^{6,9} (see SI),

which is a signature that thermal creep persists there, in agreement with recent strong pinning theory^{10,42}. At temperatures above 0.07 K strong thermal fluctuations causes the sharp jump to be replaced by a smooth evolution between the low and high resistive states⁹. Moreover, the resistance jump that is seen here only at very low T points to a collective de-pinning of the vortex-glass. Notice that Joule overheating is in play here but mainly in the resistive state above the critical current (see detailed analysis in SI).

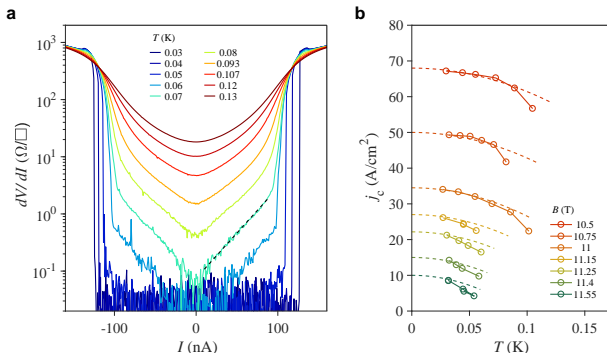


FIG. 4: **Vortex de-pinning and thermal creep.** The differential resistance dV/dI versus I of sample IT1b measured at $B = 11.25$ T at different temperatures is plotted in panel **a**. The black dashed line indicates the exponential increase of the differential resistance with the current, which is caused by vortex creep. The critical current density j_c as a function of T and B is shown in panel **b**. Each value of $j_c(B)$ was extracted from the differential resistance curves, similar to the one shown in (a), by finding the threshold to the high resistance state. Dashed lines are fits using Eq. (12) with $B_{c2}(0) = 12$ T and adjusting $j_c(T = 0, B)$ for each curve using a single prefactor for all B 's.

As we showed before, the (zero-temperature) B -dependence of the critical current scales like j_c^{GL} near $B_{c2}(0)$, indicating that $j_c^{\text{depin}} \propto j_c^{GL}$. Correspondingly, we expect the T -dependence of the critical current to be determined by the thermal corrections to the superfluid stiffness

$$\delta j_c^{GL}(T, B) \propto \frac{\delta \rho_s(T, B)}{\xi_{GL}} \propto \frac{T^2}{\sqrt{B_{c2}(0) - B}} \quad (12)$$

To test this predicted scaling of j_c as a function of temperature, we measured additional resistance curves, similar to those shown in Fig. 4a, at different magnetic fields (see SI). The critical current values near $B_{c2}(0)$ extracted from the jump in the resistance are plotted as a function of temperature in Fig. 4b. The dashed lines are fits of the $j_c(T, B)$ data to Eq. (12), which were performed by setting $B_{c2}(0) = 12.1$ T (deduced from Fig. 3), by adjusting the $T = 0$ value $j_c(0, B)$ for each B and finding one global pre-factor. We note that the resulting $j_c(0, B)$ values scale as $(B_{c2} - B)^{3/2}$. The fit reproduces remarkably well the T -dependence of the data for the $B = 10.5, 1.75$

and 11 T, confirming the T^2 correction to the critical current as well as its B -dependence. Deviations from the fit occur for the highest T data points as well as in the immediate vicinity of $B_{c2}(0)$. This is not surprising since our theoretical derivation of the correction to the superfluid stiffness given in Eq. (11) is valid so long as the fluctuations are small $\delta \rho_s(B, T) \ll \rho_s(B)$. The thermal fluctuations, however, become strong at lower T as the magnetic field is increased.

The excellent agreement between the vortex-glass fluctuation correction and the data has important implications: Together with the observation of the Ginzburg-Landau scaling of the critical current shown in Fig. 3, this analysis confirms that the collective vortex depinning, which causes the jump in the resistance, is indeed proportional to the de-pairing critical current j_c^{GL} . Moreover, this result validates our prediction for the renormalization of the superfluid stiffness by thermal fluctuations of the vortex glass, and suggests that this should affect other observables such as magnetotransport near the quantum phase transition at B_{c2} . In the following we show these fluctuations can account for the linear upturn of $B_{c2}(T)$ at low temperature.

Theory for the low-temperature anomaly

The superconducting transition in the bulk limit can be estimated from the condition $\rho_s(T, B) \approx 0$, or equivalently when $\delta \rho_s(T_c, B) = \epsilon \rho_s(0, B)$, with ϵ being a number of the order unity (similar to the Lindemann criterion for melting of solids). Under this condition and using Eqs. (4) and (11) we find

$$1 - \frac{B_{c2}(T)}{B_{c2}(0)} = C_1 \frac{\pi T}{24 \rho_{s0} a_0 \epsilon^{1/2}}, \quad (13)$$

where $C_1^2 = 4C\hbar\sigma_n a_0 / 3\pi e^2$ is of order unity for our a:InO films. In films, the transition temperature is set instead by the BKT condition:

$$\rho_s(B, T_{\text{BKT}}) = \frac{\chi}{d} T_{\text{BKT}}(B) \quad (14)$$

where d is the film thickness and χ^{-1} was numerically found⁴³ to be between 1.5 to 2.2 (this holds for *any value of* d ⁴³⁻⁴⁶). Moreover, kinetic inductance measurements of thin a:InO films have observed a universal jump in the two-dimensional superfluid density per square even in the presence of a magnetic field, indicating that the BKT transition persists near the quantum critical point¹⁴. We note that Eq. (14) in the limit $d \rightarrow \infty$ reproduces the condition for the bulk transition [$\rho_s(T, B) \approx 0$], and thus this equation describes the scaling of $B_c(T)$ for any d . Thus, combining the BKT condition with the renormalized ρ_s given by Eq. (11) yields the scaling of the transition temperature with magnetic field as a function of thickness

$$1 - \frac{B_{c2}(T)}{B_{c2}(0)} = \left[1 + \sqrt{1 + C_1^2 \frac{d^2}{\epsilon a_0^2 \chi^2}} \right] \frac{\pi \chi T}{24 \rho_{s0} d}. \quad (15)$$

We thus obtain a linear temperature dependence of $B_{c2}(T)$ at low T , which provides a theoretical description of our experimental data shown in Fig. 1b. In addition, this result is in agreement with numerous experiments in films^{3–9,12} and bulk^{10,11} disordered superconductors.

We emphasize that the linear- T dependence of $B_{c2}(T)$ does not depend on the sample dimensionality and, in particular, remains valid for bulk superconductors. For films, $|\delta\rho_s(B, T)/\rho_s(B)|$ grows with the film thickness d , however it remains much below unity so long as $d \ll a_0$ (As is the case for the experiments reported in Ref.¹²). In this thin limit our theory predicts that the slope $-dB_{c2}(T)/dT$ grows linearly with $(\rho_{s0}d)^{-1}$. For thicker films, however, $|\delta\rho_s(B, T)/\rho_s(B)|$ increases and higher order corrections to $\rho_s(B)$ can become important. Still, $dB_{c2}(T)/dT|_{T \rightarrow 0}$ maintains the structure $(\rho_{s0}a_0)^{-1}(g_0 + g_1a_0/d)$ with numerical coefficients $g_{0,1}$ that (may) deviate from those given in Eq. (15). To conclude, while our analysis provides an exact expression for the slope only in the thin-film limit, it predicts a distinct d -dependence that holds for any thickness.

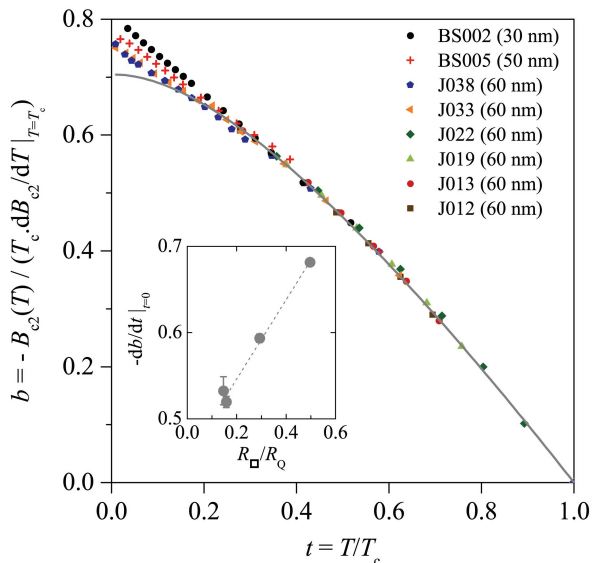


FIG. 5: **Disorder dependence of the low- T anomaly.** $b = B_{c2}(T)/(-T_c dB_{c2}/dT|_{T=T_c})$ versus reduced temperature $t = T/T_c$ for 8 samples of different thicknesses. The solid gray line is a fit using the mean field theory for dirty superconductors emphasizing the deviations at low T . Inset: Slope $-db/dt$ at zero temperature versus R_{\square}/R_Q .

Finally, we provide a quantitative comparison between the theoretical prediction and experimental data from eight samples of various thicknesses and resistances. Experimentally, the physical parameters controlling the low-temperature linear deviation are difficult to assess directly from the $B_{c2}(T)$ curves. The reduction of T_c and increase of $B_{c2}(0)$ upon increasing sheet resistance leads to an apparent increase of the slope $dB_{c2}/dT|_{T \rightarrow 0}$ in the $B - T$ plane (see fig. 2b in ref. 9). This makes a direct comparative analysis between different samples impossi-

ble. The non-universal dependence of T_c and $B_{c2}(0)$ on disorder can be eliminated by considering the quantity $b(t) = B_{c2}(T)/(-T_c dB_{c2}/dT|_{T=T_c})$ versus the reduced temperature $t = T/T_c$. Figure 5 displays $b(t)$ for the eight different samples together with the theoretical mean-field curve, in solid line, found by setting α to zero^{2,12}. We see that, for $t \gtrsim 0.2 - 0.3$, all high-temperature data collapse on the theoretical curve. At smaller t , the low-temperature anomaly of B_{c2} develops as a linear deviation from the mean-field curve. Our theory explains the anomalous slope in this regime and, as we show below, captures the dependence on the sample parameters.

To compare the plot in Fig. 5 with our theory, we extract $b(t)$ from Eq. (15) and find:

$$-\frac{db}{dt} = \begin{cases} KR_{\square}/R_Q & d \ll a_0 \\ \tilde{g}_0 \sqrt{\frac{1}{\sigma_n R_Q a_0}} + \tilde{K} \frac{R_{\square}}{R_Q} & d \gg a_0 \end{cases}, \quad (16)$$

where $R_Q = h/4e^2$ is the quantum of resistance for electron pairs (for details see the Supplementary Information). Neglecting higher order corrections to ρ_s beyond Eq. (15), and the suppression of ρ_{s0}/T_{c0} in strongly disordered superconducting films yields $K = 0.4\pi \approx 1$, $\tilde{K} \approx 0.1$, and $\tilde{g}_0 \approx 0.05\sqrt{C}$. The slopes $db(t)/dt|_{t=0}$ of four samples: 30 nm, 50 nm, and two 60 nm thick films (samples BS002, BS005, J033 and J038 respectively) are shown in the inset of Figure 5. We clearly see that the slope of the linear- T anomaly increases with sheet resistance as predicted by Eq. (16), demonstrating the consistency of our theoretical description. Furthermore, the linear dependence of $db(t)/dt|_{t=0}$ on the sheet resistance does not extrapolate to zero in the bulk limit ($d \rightarrow \infty$), confirming again our theoretical result Eq. (16). However, fitting the data to Eq. (16) gives $-db/dt = 0.4R_{\square}/R_Q + 0.44$, i.e., $\tilde{g}_0 \approx 0.45$ and $\tilde{K} \approx 0.4$. These values exceed the ones found via our simplified approximation by a factor of about 4-10. Partially, it might be due to the overestimation of the ratio ρ_{s0}/T_{c0} , see Supplementary Information. Obtaining the correct numerical coefficients presumably requires including corrections neglected above, which is beyond the scope of this work.

In conclusion, we have conducted a systematic study of the critical current near $B_{c2}(T = 0)$ in disordered a:InO films. These films are prototypical representatives of a variety of superconducting film in which the critical field shows an anomalous linear upturn as $T \rightarrow 0$. We uncovered a power-law dependence of j_c on magnetic field and extract the corresponding critical exponent. This previously unknown scaling property elucidates the origin of the 'critical field anomaly'—the strong deviation of B_{c2} from the mean-field result at the lowest temperatures. We have showed theoretically that the behavior of *both* $B_{c2}(T)$ and $j_c(B)$ can be attributed to the specific properties of the vortex-glass, which is characteristic state of disordered films in the presence of magnetic field. In particular, the anomalous dependence of B_{c2} on T is induced

by a soft overdamped (bosonic) fluctuation mode of the vortex-glass. Although this mechanism is quite generally applicable for any disordered superconductor, both 2D and 3D, the magnitude of the effect is appreciable for superconductors with low superfluid density, $\rho_s \xi_0 \leq T_{c0}$, where phase fluctuations are strong⁴⁸.

Our analysis provides sharp predictions for $B_{c2}(T)$ and $j_c(B)$ which allows a clear distinction between the physical mechanisms in play. It would be very interesting to look for similar scaling in other superconducting films (in particular amorphous/non-amorphous) where a similar B_{c2} anomaly has been observed^{3-8,10-12}. A detailed measurement of the thickness and field dependence of the critical current could shed light on difference and similarities of the vortex-glass phases in conventional and also unconventional superconductors.

Methods

Sample fabrication and measurement setup.

Disordered a:InO films were prepared by e-gun evapo-

ration of 99.99 % In₂O₃ pellets on a Si/SiO₂ substrate in a high-vacuum chamber with a controlled O₂ partial pressure. Films were patterned into Hall bar geometry (100 μm wide for all samples except ITb1 which is 20 μm wide) by optical lithography, enabling four-terminal transport measurements using standard low-frequency lock-in amplifier and DC techniques. Measurements were performed in dilution refrigerators equipped with superconducting solenoid. Multi-stage filters, including feed-through π -filters at room temperature, highly dissipative shielded stainless-steel twisted pairs down to the mixing chamber, copper-powder filters at the mixing chamber stage, and 47 nF capacitors to ground on the sample holder, were installed on each dc lines of the fridge. This careful filtering of low and high frequency noises was crucial to measure well defined critical currents as low as ~ 50 nA (see Fig. 4), which would have been otherwise disguised by spurious noise. Furthermore, a calibrated RuO₂ thermometer was installed directly on the sample holder to precisely monitor the sample temperature. This accurate thermometry eliminates small temperature gradients below 0.1 K.

-
- ¹ Abrikosov, A. A. and Gor'kov, L. P. Contribution to the theory of superconducting alloys with paramagnetic impurities. *Zh. Eksp. Teor. Fiz.* **39**, 1781 (1960) [*Sov. Phys. JETP* **12**, 1243 (1961)].
- ² Maki, K. Critical Fluctuation of the Order Parameter in a Superconductor. I. *Prog. Theor. Phys.* **40**, 193–200 (1968).
- ³ Tenhover, M. and Johnson and W. L. and Tsuei, C. C. Upper critical fields of amorphous transition metal based alloys. *Solid State Commun.* **38**, 53–57 (1981).
- ⁴ Okuma, S. and Komori, F. and Ootuka, Y. and Kobayashi, S.-I. Superconducting properties of disordered films of Zn. *J. Phys. Soc. Jpn.* **52**, 2639–2641 (1983).
- ⁵ Hebard, A. F. and Paalanen, M. A. Pair-breaking model for disorder in two-dimensional superconductors. *Phys. Rev. B* **30**, 4063–4066 (1984).
- ⁶ Graybeal, J. M. and Beasley, M. R. Localization and interaction effects in ultrathin amorphous superconducting films. *Phys. Rev. B* **29**, 4167–4169 (1984).
- ⁷ Furubayashi, T. and Nishida, N. and Yamaguchi, M. and Morigaki, K. and Ishimoto, H. Superconducting properties of amorphous $\text{Si}_{1-x}\text{Au}_x$ near metal-insulator transition. *Solid State Commun.* **55**, 513–516 (1985).
- ⁸ Nordström, A. and Dahlborg, U. and Rapp, Ö. Variation of disorder in superconducting glassy metals. *Phys. Rev. B* **48**, 12866–12873 (1993).
- ⁹ Sacépé, B. and Seidemann, J. and Ovidia, M. and Tamir, I. and Shahar, D. and Chapelier, C. and Strunk, C. and Piot, B. A. High-field termination of a Cooper-pair insulator. *Phys. Rev. B* **91**, 220508(R) (2015).
- ¹⁰ Ren, Z. and Kriener, M. and Taskin, A. A. and Sasaki, S. and Segawa, K. and Ando, Y. Anomalous metallic state above the upper critical field of the conventional three-dimensional superconductor AgSnSe_2 with strong intrinsic disorder. *Phys. Rev. B* **87**, 064512 (2013).
- ¹¹ Bustarret, E. and Kačmarčík, J. and Marcenat, C. and Gheeraert, E. and Cytermann, C. and Marcus, J. and Klein, T. Dependence of the Superconducting Transition Temperature on the Doping Level in Single-Crystalline Diamond Films. *Phys. Rev. Lett.* **93**, 237005 (2004).
- ¹² Xing, Y. and Zhang, H.-M. and Fu, H.-L. and Liu, H. and Sun, Y. and Peng, J.-P. and Wang, F. Lin, X. and Ma, X.-C. and Xue, Q.-K. and Wang, J. and Xie, X. C. Quantum Griffiths singularity of superconductor-metal transition in Ga thin films. *Science* **350**, 542 (2015).
- ¹³ Spivak, B. and Zhou, F. Mesoscopic Effects in Disordered Superconductors near H_{c2} . *Phys. Rev. Lett.* **74**, 2800–2803 (1995).
- ¹⁴ Galitski, V. M. and Larkin, A. I. Disorder and Quantum Fluctuations in Superconducting Films in Strong Magnetic Fields. *Phys. Rev. Lett.* **87**, 087001 (2001).
- ¹⁵ Coffey, L. and Levin, K. and Muttalib, K. A. Upper critical field of strongly disordered three-dimensional superconductors: Localization effects. *Phys. Rev. B* **32**, 4382–4391 (1985).
- ¹⁶ Sadovskii, M. V. Superconductivity and localization. *Phys. Rep.* **282**, 225–348 (1997).
- ¹⁷ Smith, R. A. and Handy B. S. and Ambegaokar, V. Upper critical field in disordered two-dimensional superconductors. *Phys. Rev. B* **61**, 6352–6359 (2000).
- ¹⁸ H. Kim, A. Ghimire, S. Jamali, T.K. Djidjou, J.M. Gerton, and A. Rogachev, Effect of magnetic Gd impurities on the superconducting state of amorphous Mo-Ge thin films with different thickness and morphology, *Phys. Rev. B* **86**, 024518 (2012).
- ¹⁹ Galitski, V. M. and Larkin, A. I. Superconducting fluctuations at low temperature. *Phys. Rev. B* **63**, 174506 (2001).
- ²⁰ Galitski, V. Nonperturbative Microscopic Theory of Superconducting Fluctuations near a Quantum Critical Point. *Phys. Rev. Lett.* **100**, 127001 (2008).
- ²¹ Welp, U and Kwok, W. K. and Crabtree, G. W. and Van-

- dervoort, K. G. and Liu, J. Z. Magnetic measurements of the upper critical field of $YBa_2Cu_3O_{7-\delta}$ single crystals. *Phys. Rev. Lett.* **62**, 1908-1911 (1989).
- ²² Golubov, A. A. and Dorin, V. V. The upper critical field of thin superconducting films with large resistance. *J. Low Temp. Phys.* **78**, 375-386 (1990).
- ²³ Mikitik, G. P. Temperature dependence of the upper critical field of type II superconductors with fluctuation effects. *Zh. Eksp. Teor. Fiz.* **101**, 1042-1055 (1992) [*Sov. Phys. JETP* **74**, 558-564 (1992)].
- ²⁴ Osofsky, M. S. and Soulen, Jr., R. J. and Wolf, S. A. and Broto, J. M. and Rakoto, H. and Ousset, J. C. and Coffe, G. and Askenazy, S. and Pari, P. and Bozovic, I. and Eckstein, J. N. and Virshup, G. F. Anomalous temperature dependence of the upper critical magnetic field in Bi-Sr-Cu-O. *Phys. Rev. Lett.* **71**, 2315-2318 (1994).
- ²⁵ Park, T. and Ronning, F. and Yuan, H. Q. and Salamon, M. B. and Movshovich, R. and Sarrao, J. L. and Thompson, J. D. Hidden magnetism and quantum criticality in the heavy fermion superconductor $CeRhIn_5$. *Nature* **440**, 65-68 (2006).
- ²⁶ Berezinskii, V. L. Destruction of long-range order in one-dimensional and two-dimensional systems having a continuous symmetry group I. Classical systems. *Zh. Eksp. Teor. Fiz.* **59**, 907-920 (1970) [*Sov. Phys. JETP* **32**, 493-500 (1971)].
- ²⁷ Kosterlitz, J. M. and Thouless, D. J. Long range order and metastability in two dimensional solids and superfluids. (Application of dislocation theory). *J. Phys. C: Solid State Phys.* **5**, L124 (1972).
- ²⁸ Larkin, A. I. and Ovchinnikov, Yu. N. Collective Pinning. *Physica B+C* **126**, 187-192 (1984).
- ²⁹ Blatter, G. and Feigel'man, M. V. and Geshkenbein, V. B. and Larkin, A. I. and Vinokur, V. M. Vortices in high-temperature superconductors. *Rev. Mod. Phys.* **66**, 1125-1388 (1994).
- ³⁰ Kwok, W.-K. and Welp, U. and Glatz, A. and Koshelev, E. and Kihlstrom, K. J. and Crabtree, G., Vortices in high-performance high-temperature superconductors, *Rep. Progr. Phys.* **79**, 116501 (2016)
- ³¹ Mkrtchyan, G.S. and Shmidt V. V., Interaction between a cavity and a vortex in a superconductor of the second kind, *Sov. Phys. JETP* **34**, 195 (1972).
- ³² Fisher, D. S. and Fisher, M. P. A. and Huse, D. A. Thermal fluctuations, quenched disorder, phase transitions, and transport in type-II superconductors. *Phys. Rev. B* **43**, 130-159 (1991).
- ³³ Sacépé, B., Dubouchet, T., Chapelier, C., Sanquer, M., Ovdadia, M., Shahar, D., Feigel'man & M., Ioffe, L. Localization of preformed Cooper pairs in disordered superconductors. *Nature Phys.* **7**, 239-244 (2011).
- ³⁴ Feigel'man, M. V. and Ioffe, L. B. and Kravtsov V. E. and Cuevas, E. Fractal superconductivity near localization threshold. *Ann. Phys.* **325**, 1390-1478 (2010).
- ³⁵ Campbell, A. M. The response of pinned flux vortices to low-frequency fields. *J. Phys. C: Solid State Phys.* **2**, 1492 (1969).
- ³⁶ Campbell, A. M. The interaction distance between flux lines and pinning centres. *J. Phys. C: Solid State Phys.* **4**, 3186 (1971).
- ³⁷ Coffey, M. W. and Clem, J. R. Unified theory of effects of vortex pinning and flux creep upon the rf surface impedance of type-II superconductors. *Phys. Rev. Lett.* **67**, 386 (1991).
- ³⁸ Willa, R. and Geshkenbein, V. B. and Blatter, G. Probing the pinning landscape in type-II superconductors via Campbell penetration depth. *Phys. Rev. B* **93**, 064515 (2016).
- ³⁹ Strnad, A. R. and Hempstead, C. F. and Kim, Y. B. Dissipative Mechanism in Type-II Superconductors *Phys. Rev. Lett.* **13**, 794-797 (1964).
- ⁴⁰ Xiao, Z. L. and Andrei, E. Y. and Paltiel, Y. and Zeldov, E. and Shuk, P. and Greenblatt, M. Edge and bulk transport in the mixed state of a type-II superconductor *Phys. Rev. B* **65**, 094511 (2002).
- ⁴¹ Thomann, A. U. and Geshkenbein, V. B. and Blatter, G. Dynamical Aspects of Strong Pinning of Magnetic Vortices in Type-II Superconductors. *Phys. Rev. Lett* **108**, 217001 (2012).
- ⁴² Buchacek, M., and Willa, R., and Geshkenbein, V. B., and Blatter, G., Thermal depinning and creep in strong pinning theory, arXiv:1802.00652 (2018).
- ⁴³ Schneider, T. and Schmidt, A. Dimensional Crossover Scaling in the Layered xy-Model and ^4He Films. *J. Phys. Soc. Jpn.* **61**, 2169-2172 (1992).
- ⁴⁴ Ambegaokar, V. and Halperin, B. I. and Nelson, D. R. and Siggia, E. D. Dynamics of superfluid films. *Phys. Rev. B* **21**, 1806-1826 (1980).
- ⁴⁵ Williams, G. A. Dimensionality crossover of the ^4He superfluid transition in a slab geometry. *J. Low. Temp. Phys.* **101**, 415-420 (1995).
- ⁴⁶ Schultka, N. and Manousakis, E. Crossover from two- to three-dimensional behavior in superfluids. *Phys. Rev. B* **51**, 11712-11720 (1995).
- ⁴⁷ Misra, S. and Urban, L. and Kim, M. and Sambandamurthy, G. and Yazdani, A. Measurements of the Magnetic-Field-Tuned Conductivity of Disordered Two-Dimensional $\text{Mo}_{43}\text{Ge}_{57}$ and InO_x Superconducting Films: Evidence for a Universal Minimum Superfluid Response *Phys. Rev. Lett.* **110**, 037002 (2013).
- ⁴⁸ Emery, V. J. and Kivelson, S. A. Importance of phase fluctuations in superconductors with small superfluid density. *Nature*, **374**, 6521 (1995).

Acknowledgments We are grateful to Vadim Geshkenbein, Lev Ioffe, Thierry Klein and Mikhail Skvortsov for useful discussions. We thank Idan Tamir and Dan Shahar for providing sample ITb1. This work was supported by the Lab Alliance for Nanosciences and Energies for the Future (Lanef) and the H2020 ERC grant *QUEST* No. 637815. Research of M.V.F. was partially supported by the Russian Science Foundation grant # 14-42-00044.

Supplementary Information of Quantum meets classical phase transition: Low-temperature anomaly in disordered superconductors near B_{c2}

I. SAMPLE PARAMETERS

Table S1 provides the thickness, sheet resistance before superconducting transition, and critical temperature determined by a 50% drop in the normal state resistance for all the a:InO samples studied in this work. MoGe030 is an amorphous molybdenum-germanium (MoGe) thin film that has been deposited by magnetron sputtering from Mo78Ge22 composite target fabricated KJ Lesker company. We used Si substrate covered with a 60-nm-thick layer of SiN grown by chemical vapor deposition. Prior to the deposition of the MoGe film, a 3-nm-thick underlayer of amorphous Ge was deposited. This underlayer is critical for the growth of the homogeneous MoGe films¹. For oxidation protection the films were covered by a 10-nm-thick layer of Ge. All layers were deposited without breaking vacuum (base value 5×10^{-8} Torr) via the same shadow mask made in thin stainless steel plate.

Sample	d (nm)	R_{\square}^{max} ($k\Omega$)	T_c (K)
J012	60	0.5	3.5
J013	60	0.7	3.4
J019	60	1.3	3.1
J022	60	2.3	2.7
J033	60	1.3	3.2
J038	60	1.2	3.5
BS005	50	2.2	2.6
BS002	30	3.5	2.4
ITb1	30	2.5	3.0
MoGe030	3	0.7	4.0

TABLE S1: Sample parameters. Thickness, d , was measured by atomic force microscopy; R_{\square}^{max} is the maximum sheet resistance reached before the superconducting transition. T_c is the superconducting critical temperature.

II. AMORPHOUS MOLYBDENUM-GERMANIUM THIN FILM

To test the universality of our results on the anomalous dependence of the critical magnetic field on temperature, we repeated the measurements on another material, that is, amorphous molybdenum-germanium (MoGe), whose parameters are given in Table S1. Figure S1a displays the magnetoresistance curves of this sample measured at different temperatures. Similar to the case of the a:InO samples, the transition to the normal state becomes steeper upon decreasing temperature, indicating strong vortex pinning. The temperature dependence of the critical field, $B_{c2}(T)$, extracted from these magnetoresistance data at 50% of the normal state resistance is shown in Fig. S1b together with a fit of the mean-field theory of dirty superconductors^{12,13}. A clear low- T anomaly develops below 0.6 K with a nearly linear increase of $B_{c2}(T)$ on lowering further the temperature.

We then performed systematic measurements of the critical current in the MoGe sample near $B_{c2}(0)$. The results are shown in Fig. S1c which presents the critical current density j_c as a function of $B_c^{j_c} - B$. For $B_c^{j_c} = 7$ T, most of the data collapse on a straight line which is denoted by the red line of slope 3/2. This collapse is in agreement with our previous experimental findings, which are reported in the main text, i.e., the mean-field scaling $j_c \propto (B_c^{j_c} - B)^{3/2}$. The scattering of the data, in particular below the red line, is a consequence of sample heating by the large current in the resistive state (see section IV). When the thermalization time in the superconducting state is not long enough while sweeping the current, the critical current is reduced compared to its zero temperature limit.

To conclude, the study of a second material consistently confirms that, in disordered thin films, the de-pinning critical current is proportional to the de-pairing current with a mean-field scaling $j_c \propto (B_c^{j_c} - B)^{3/2}$. Moreover, the data obtained for the MoGe film demonstrate the generality of our explanation for the origin of the low- T anomaly of the critical field.

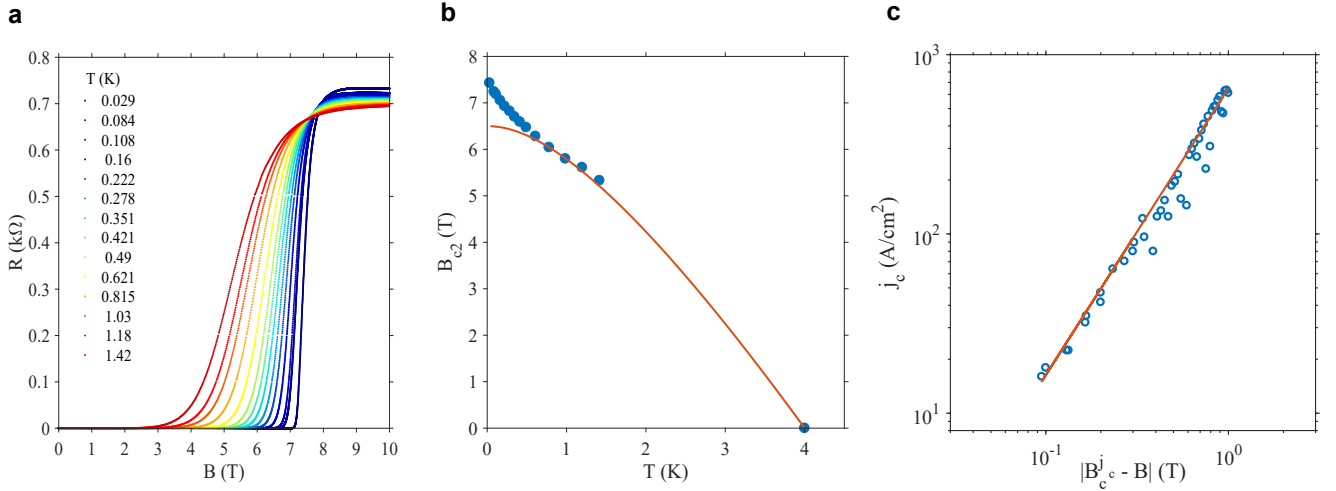


FIG. S1: **MoGe thin film.** **a**, Magnetoresistance curves measured at different temperatures with an excitation current of 1 nA. **b**, B_{c2} versus T extracted from **a** at 50% of normal state resistance. The red line is a fit with the theory of dirty superconductors. **c**, Critical current density j_c versus $B_c^j - B$ with $B_c^j = 7$ T. The red line is a guide for the eyes of slope $3/2$.

III. DIFFERENTIAL RESISTANCE

In this section we present the full set of data used to extract the temperature dependence of the critical current as shown in Fig. 4b of the main text. Figure S2 displays the differential resistance dV/dI curves versus current, measured at different temperatures and magnetic fields. The applied dc current was swept from negative to positive values while measuring the differential resistance with a lockin amplifier technique and an ac current modulation of 1 nA. Temperature was carefully monitored with an on-chip thermometer (see Methods). For all set of curves, a resistance jump develops at low temperature for a given current threshold. This current threshold is slightly hysteretic, that is, depends on the direction of current sweep. In this work, the critical current is identified as the current threshold on the switching to the resistive state at positive current values. Below the critical current, the differential resistance exhibits an exponential increase with the applied current. This exponential increase persists even at high temperatures when the jump is absent and replaced by a smeared crossover to the resistive state.

The exponential increase of the differential resistance in our films relates to vortex creep. Vortex motion is apparent in the temperature dependence of the resistance at zero bias shown in Fig. S3, which exhibits an activated behavior down to our lowest temperature. This activation at zero bias results from thermally assisted flux-flow with a barrier $U(B)$ that is a function of the magnetic field. At non-zero bias, the Lorentz force applied to the vortices by the driving current reduces the activation barrier in the following way:²

$$U(B, j) = U(B) \left(1 - \frac{j}{j_1} \right), \quad (17)$$

where $j_1 = \frac{\zeta U(B)}{\xi^2 d B L}$ is a current density related to the superconducting coherence length ξ , the thickness d and the distance between two potential wells L (ζ being a constant). As a result, the differential resistance grows exponentially with *both* T and j ,

$$R(T, j) = R_0 e^{-U(B, j)/T}. \quad (18)$$

This vortex creep picture describes very well our data in which a systematic exponential increase of the differential resistance on increasing current is invariably observed at low temperatures below the critical current.

To investigate the I - V characteristics above the critical current, we numerically integrated the differential resistance curves shown in Fig. 4a of the main text. The resulting I - V 's are shown in Fig. S4. At the lowest temperatures, a non-zero voltage sets in above the critical current and then raises linearly on increasing further the bias current. This linear I - V curves indicate an ohmic regime of flux-flow that is shifted by an excess current offset corresponding to the critical current. Such peculiar behavior were observed earlier in various disordered superconductors⁶⁻⁹ and have been

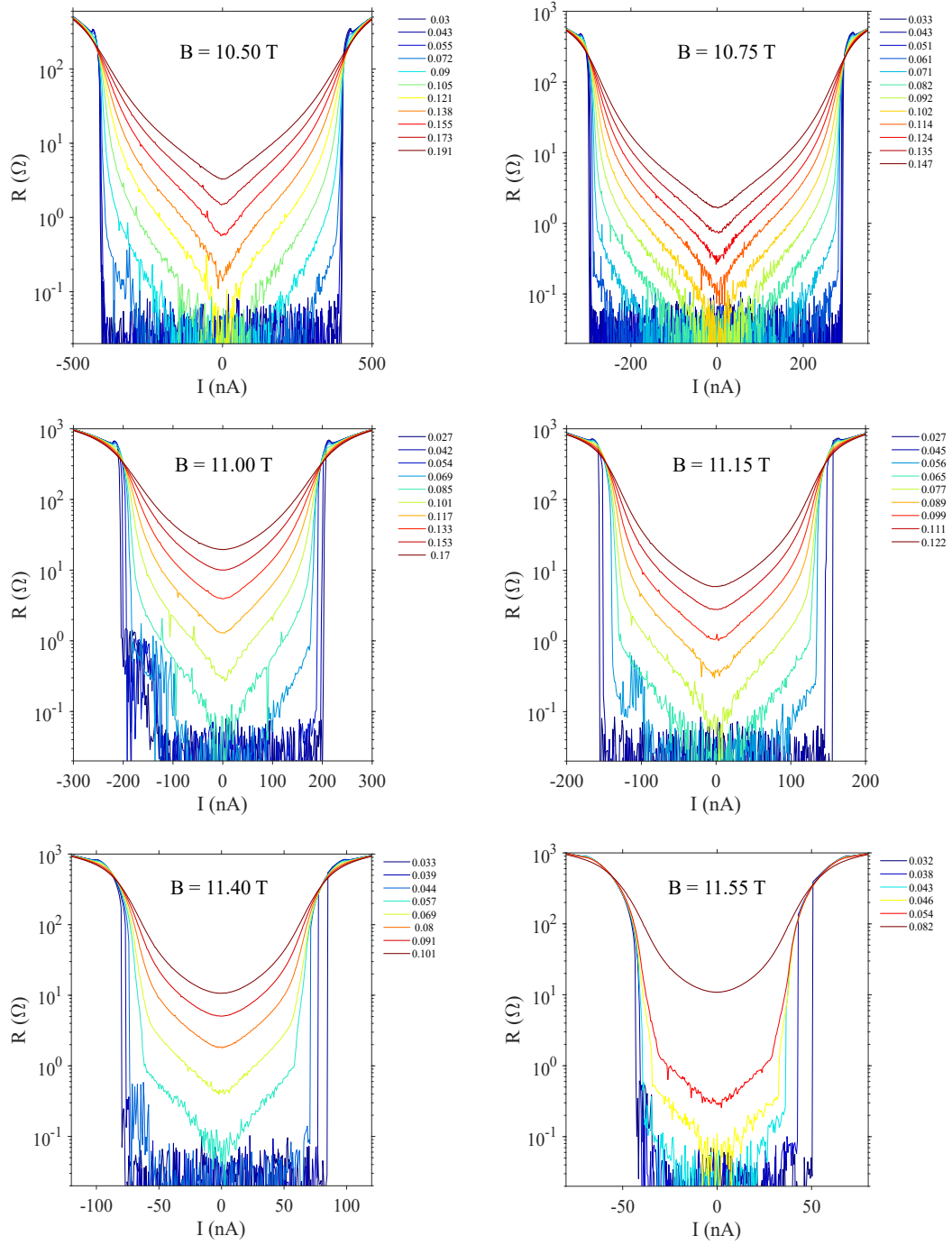


FIG. S2: dV/dI curves versus applied current I for various temperatures and magnetic fields on sample ITb1. Current is systematically swept from negative to positive values.

recently interpreted as a signature of vortex creep persisting beyond the critical current when vortices are strongly pinned^{10,11}.

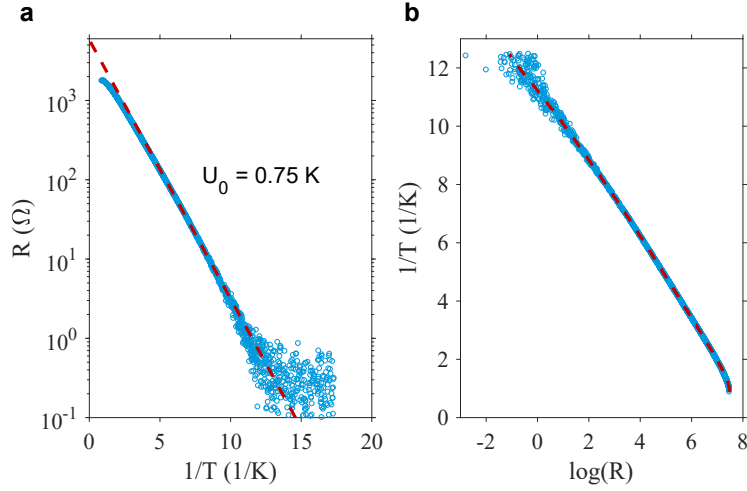


FIG. S3: **Thermally assisted flux creep.** **a**, Arrhenius plot of the resistance at $B = 11.25$ T. The red dashed line is an Arrhenius fit giving an activation energy of $U_0 = 0.75$ K and a prefactor of $5.8 k\Omega$. **b**, Same data but with a polynomial fit that is used as the electron temperature thermometer.

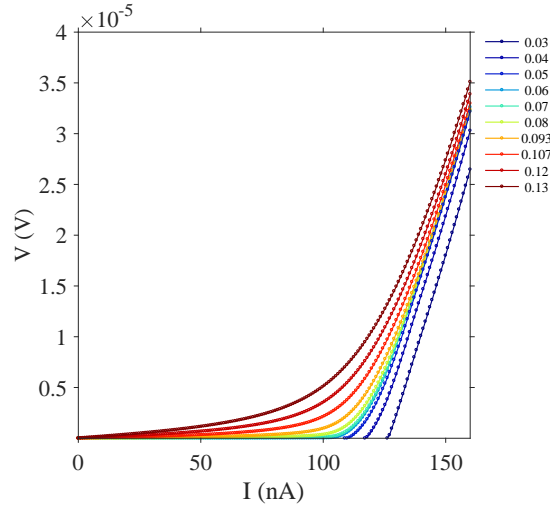


FIG. S4: **Excess current.** I - V characteristics obtained after numerical integration of the data of Fig. 4a of the main text. The resistive state extrapolates linearly at $V = 0$ to the critical current.

IV. JOULE OVERHEATING SCENARIO

Joule heating is ubiquitous in non-equilibrium measurements. At low temperature, when the electron-phonon coupling is weak, dissipation due to an applied bias can potentially induce electron-overheating and subsequently, non-linear I - V characteristics³. This is particularly true with disordered conductors when the resistance is large and exhibits a diverging temperature dependence due to transition into insulating or superconducting states. In disordered insulators, such as the high field regime of the B -induced insulator in a:InO films, non-linearities in the I - V 's mainly stem from electron-overheating^{4,5}. At very low T , when the bias voltage V reaches a voltage threshold V_{th} , these non-linear I - V 's exhibit a hysteretic current jump of several orders of magnitudes between a high resistive state at $V < V_{th}$ and a low resistive state at $V > V_{th}$. The hysteresis and current jump have been proven to be a direct consequence of a thermal bistability of the electronic system driven by Joule overheating^{4,5}.

In this section we address the possibility that the resistance jumps and the accompanying non-linearities we observe near $B_{c2}(0)$ in our moderately disordered superconducting a:InO films result from a similar electron overheating and thermal bistability. For this purpose, we analyze the heat balance equation^{4,5}:

$$P = R(T_{el}) \times I^2 = \Gamma \Omega (T_{el}^\alpha - T_{ph}^\alpha), \quad (19)$$

where Γ is the electron-phonon coupling constant, Ω the sample volume, T_{ph} is the phonon bath temperature as measured by the on-chip thermometer, and α the exponent describing the electron-phonon heat transfer. The left-hand-side of the equation describes the heat pumped into the electronic system by the applied current, while the right-hand-side corresponds to the heat dissipated to the lattice due to electron-phonon interactions. Since $R(T_{el})$ is a steep function of the temperature near $B_{c2}(T)$ (see Eq. (18)), a small change in T_{el} yields a large change in the resistance and hence, a significant non-linearity in the I - V . Next, we follow the analysis of Ref. 4: Using the experimental data for $R(T_{el})$ and the I - V curves, we find the electrons temperature as a function of the current. To extract the temperature, we assume that $R(T_{el})$ is a smooth exponential function of the temperature, as measured at low current. Finally, we check that the calculated T_{el} satisfies the heat balance equation (Eq. 19). If the later is correct, the jump in the resistance can be attributed to heating effects, and the critical current is not a property of the superconducting state.

A. Heating analysis of the data at $B = 11.25$ T

We demonstrate the analysis of the heat balance equation on the data presented in Fig. 4a, which was measured at $B = 11.25$ T. We start by numerically integrating the dV/dI curves to extract the voltage drop across the sample. Figure S5 displays the resulting I - V 's in a semilog scale for different temperatures. Notice that although no voltage jump is observed at $T = 0.06$ K, we still find a resistance jump (see Fig. 4a). For the lowest T , the integrated voltage below the current threshold is not shown since the differential resistance measurement remains below the noise level of our apparatus. A polynomial fit of the zero-bias resistance curve, $R_{I \rightarrow 0}(T_{el} = T_{ph})$, shown in Fig. S3 is used to extract the electronic temperature as a function of the current for each I - V curve. The resulting T_{el} versus current curves are presented in Fig. S5b. The effective electronic temperature raises by a factor two once the film transfer into the resistive state above the critical current.

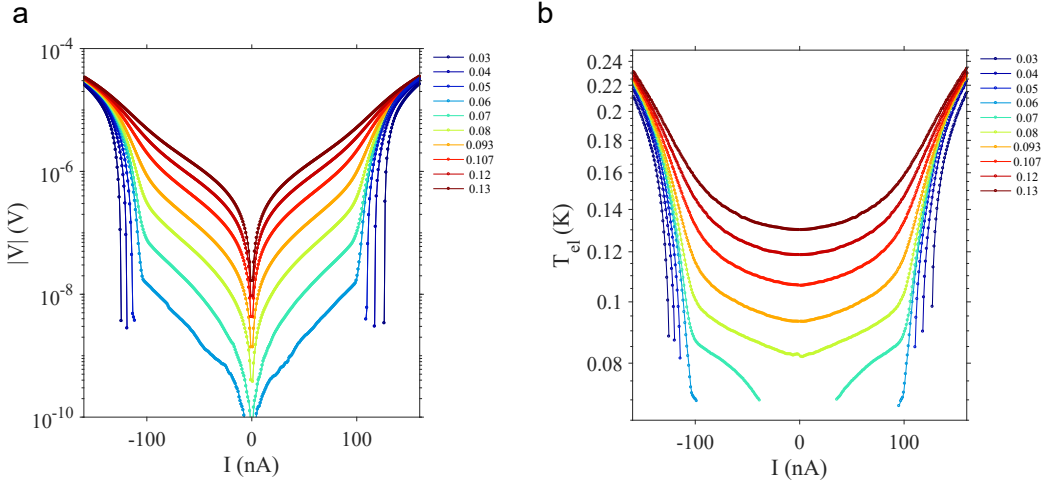


FIG. S5: **Effective electronic temperature.** **a**, $|V|$ versus I for different phonon temperatures. The voltage is obtained by numerical integration of the dV/dI curves of Fig. 4a. **b**, Effective electronic temperature T_{el} versus I , extracted from **a** and the measured $R(T)$ curves of Fig. S3.

We turn to computing the dissipated power P for each I - V , and we plot it as a function of T_{el} in Fig S6a. The resulting curves collapse at high power and high T_{el} , i.e., in the resistive state above the critical current. Such a collapse is typically an indication that some electron overheating takes place in this regime. Furthermore, it enables us to assess the exponent α of the heat balance equation (19). We find $\alpha \simeq 5.5$, which is slightly different from $\alpha = 6$ found in the high field regime of the B -induced insulator of a:InO films near the superconductor-insulator transition⁴. To self-consistency check the heat balance, we plot in Fig. S6b the power P as a function of $T_{el}^{5.5} - T_{ph}^{5.5}$. In case of a purely heating-related non-linearities, we expect a collapse of all data on a straight line of slope 1 which confirms the heat balance equation. The resulting plot displayed in Fig. S6b displays a collapse of the data at $P > 10^{-13}$ W on a straight line of slope 1 (the dashed line is a guide for the eyes with a slope 1) similar to that in Fig S6a. Inspecting Fig. S5a, we obtain that this collapse occurs at voltage and current ranges ($\geq 1 \mu\text{V}$ and ≥ 100 nA) that are well above the resistance jump (or the steep increase replacing the jump at high T). For $P < 10^{-13}$ W, however, the data conspicuously does not collapse. This demonstrates the breakdown of the heating scenario and/or the assumption of

intrinsic linearity of the system in the low- P regime of the data. We note that small variation of α in this plot does not enable to recover a collapse of the low-power data.

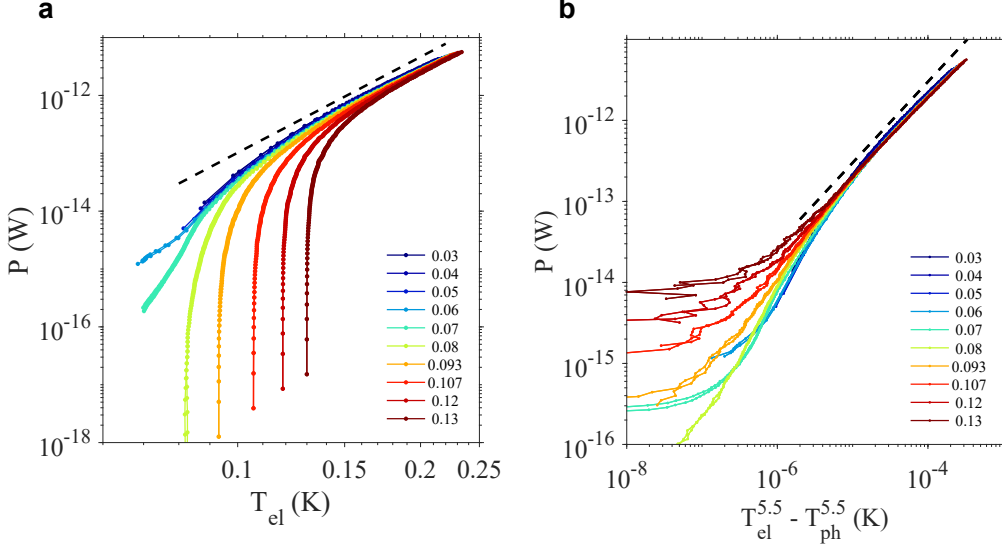


FIG. S6: **Heat balance self-consistency check.** **a**, Dissipated power P versus T_{el} for different T_{ph} 's. The high T_{el} and P regime of these curves provides an estimate of the exponent α of the heat balance equation (19). **b**, P versus $T_{el}^{5.5} - T_{ph}^{5.5}$.

B. Vortex creep below the critical current versus heating scenario

The combination of an exponentially suppressed zero-bias resistance (Eq. (18)) and the heat balance equation (19) can lead to a thermal bistability, and consequently a voltage jump as a function of the current. In this section, we show that such bistability cannot describe the resistance jump observed in the vicinity of $B_{c2}(0)$ in our samples, nor the sub-critical current resistance that we attribute, instead, to vortex creep. We apply here a reverse analysis similar to that performed in Ref.⁴ for the insulating state: We numerically calculate the I - V curves directly from the heat balance equation (19) as well as the T -dependence of the zero-bias resistance. The latter is approximated by Eq. (18) that describes very well the data in the low- T range (see Fig. S3a). From the high power data in Fig. S6, we obtain $\Gamma = 0.36 \text{ nW}/\mu\text{m}^3/\text{K}^{5.5}$ for the approximate volume $\Omega = 24 \mu\text{m}^3$. We then solve the heat balance equation for the experimental phonon bath temperatures corresponding to the $B = 11.25 \text{ T}$ measurement and obtain T_{el} as a function of I as shown in Fig. S7a. The order of magnitude of overheating agrees with the previous analysis in Fig. S5b for the high T_{ph} curves and at high current bias. The I - V curves can be straightforwardly computed from the relation $V = R(T_{el}) \times I$. The result shown in the semi-logarithmic plots of Fig. S7b and c leads to three important conclusions. First, the calculated I - V 's are hysteretic with a switching and retrapping currents whose order of magnitude agrees with the data at $T_{ph} \geq 0.06 \text{ K}$. Notice that switching (retrapping) current is defined at the transition from the low (high) resistance state to the high (low) resistance state. Second, the retrapping current is constant, independent of T_{ph} , whereas it increases on decreasing T_{ph} in the actual experimental data (see Fig. 4a of the main text and Fig. S2). Third, the switching current increases with decreasing T_{ph} much more rapidly than the data.

The agreement between data and simulations for $T_{ph} \geq 0.06 \text{ K}$ confirms the analysis of the previous section where the heat balance equation was reproduced by the data at high power (Fig. S6). However, the voltage jumps seen in these simulations, which result from thermal bistability similar to that found in the insulator^{4,5}, clearly do not match with the resistance jump observed experimentally. One key difference is the constant retrapping current in the simulation (independent of T_{ph}), which results from the fact that, when sweeping the current from the resistive state to zero-bias, the electron bath is overheated to a temperature $T_{el} > T_{ph}$ that is independent of T_{ph} . In the data of Fig. 4a and Fig. S2, the retrapping current increases when T_{ph} is lowered, indicating that another mechanism, namely vortex depinning, is in play and drives the resistance jump. Still the small asymmetry between retrapping and switching currents in the data is most likely a residual effect of overheating in the resistive state that decreases the value of the critical current at the retrapping current. At last, the fact that the simulation fails to reproduce the switching current for $T_{ph} < 0.06 \text{ K}$ —the computed switching current diverges much faster than the data—further

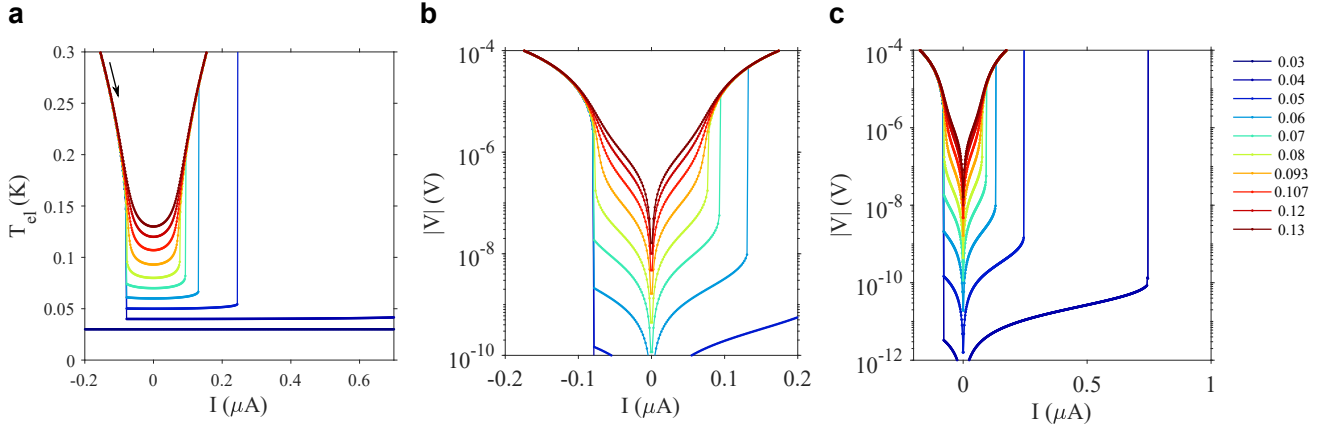


FIG. S7: **Numerically computed I - V 's.** **a**, T_{el} versus I computed from the heat balance equation (19) and the thermally assisted flux flow equation (18) that describe the low- T dependence of the zero-bias $R(T)$. The black arrow indicates the direction of sweep that defines the polarities of retrapping and switching currents. **b**, resulting I - V 's computed with $V = R(T_{el}) \times I$. **c**, same as in **b** but in a larger scale to emphasize the divergence of the switching current at low temperature.

demonstrates that the resistance jump does not result from a thermal bistability.

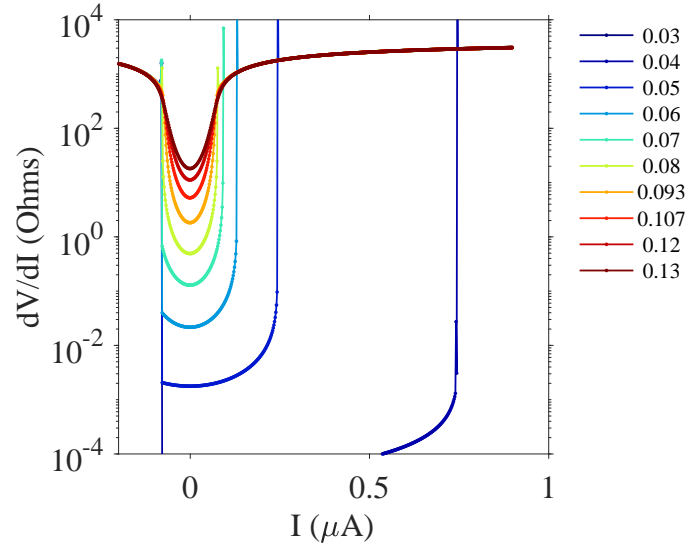


FIG. S8: **Numerically computed differential resistance.** **a**, dV/dI versus I computed from the I - V data of Fig. S7.

We finish our discussion on a last but major difference between the simulated I - V 's and the data. Below the critical current, an exponential increase of the differential resistance with the applied current is systematically observed in our data (see Fig. 4a and Fig. S2). We show in Fig. S8 the differential resistance dV/dI numerically computed from the simulations shown in Fig. S7. We clearly see that, below the switching current, the dependence of the differential resistance on applied current is not exponential at all, marking a stark difference with the data.

In conclusion, the non-linearities in the I - V 's in the superconducting state near $B_{c2}(0)$ are intrinsic and results from the vortex glass state. The exponential increase of the resistance below j_c is the signature of vortex creep and the resistance jump signals depinning of the vortex glass. Overheating is still present in the resistive state at large current but does not affect the vortex physics below the critical current. At high bias above the critical current, it is not clear however how to disentangle heating effects with thermal creep interpretation that has been put forward recently^{10,11}. The role of dissipation in this high current regime deserves further theoretical and experimental attention that goes beyond the scope of this work.

C. Magnetic field dependence of the thermal bistability scenario

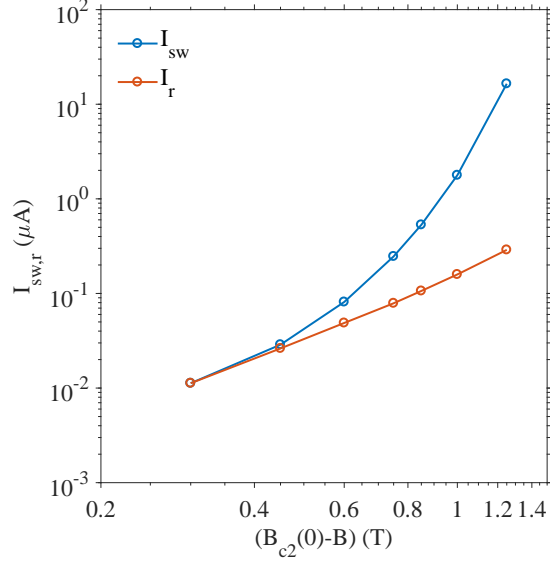


FIG. S9: **Switching and retrapping currents on approaching $B_{c2}(0)$.** Switching and retrapping currents, I_{sw} and I_r , versus $B_{c2}(0) - B$ computed from the I - V 's and the $R(T)$ data at various magnetic field values and $T_{ph} = 0.05$ K. Parameters of the heat balance equation are the same as in the previous section.

We show in this section the evolution of the switching current with magnetic field $B \approx B_{c2}(0)$ within the heating scenario. For this purpose, we repeat the previous analysis: We first fit the zero-bias $R(T)$ curves with Eq. (18) for different values of B in the vicinity of $B_{c2}(0)$. This enables us to compute the switching and retrapping currents at a fixed $T_{ph} = 0.05$ K as a function of B and check if the switching and retrapping currents induced by the thermal bistability can mimic the mean-field scaling $j_c \propto (B_{c2}(0) - B)^{3/2}$. The result is shown in Fig. S9 which displays the switching and retrapping currents as a function of $B_{c2}(0) - B$. We see that the retrapping current scales as a power of $B_{c2}(0) - B$ with an exponent $\simeq 2.2$, but the switching current does not. This, again, demonstrates that the thermal bistability interpretation cannot account for the resistance jump nor for the mean-field scaling of the critical current that has been observed in this work.

V. DERIVATION OF THE NORMALIZED SLOPE $db(t)/dt|_{t \rightarrow 0}$.

Here we present the transformation between Eq.(15) and Eq.(16) of the main text. Inserting Eq.(15) into $b(t) = B_{c2}(T)/(-T_c dB_{c2}/dT|_{T=T_c})$ yields

$$\frac{b(0) - b(t)}{t} = \left[1 + \sqrt{1 + \frac{C_1^2 d^2}{\epsilon a_0^2}} \right] \frac{\pi \chi}{24 \rho_{s0} d} \frac{B_{c2}(0)}{|dB_{c2}/dT|_{T=T_c}}. \quad (20)$$

It remains only to determine B_{c2} in two limits, $T \rightarrow 0$ and $T \rightarrow T_c$, starting with the latter. As discussed in the main text, the transition in the films is of the BKT type with the condition $\rho_s(T, B_c) = \chi T/d$. Near T_c the superfluid stiffness of a disordered superconductor is given by¹³

$$\rho_s(T, B) = \frac{\pi \sigma_n \hbar}{8 T e^2} |\Delta(T, B)|^2. \quad (21)$$

The gap $\Delta(T, B)$ near T_c can be found by minimizing the free energy in Eq.(2) of the main text, without the gradient term: $|\Delta|^2 = \alpha/2\beta$. Here α is given by Eq.(3) of the main text, which we expand to first order in B , and $\beta = \nu \psi^{(2)}(1/2)/32\pi^2 T^2$ [$\psi^{(2)}(x) = d^2\psi(x)/dx^2$ is the second derivative of the digamma function]. Thus, in this limit

the superfluid stiffness as a function of temperature and magnetic field is

$$\rho_s(T, B) = \frac{2\pi^2 T \sigma_n \hbar}{e^2 \psi^{(2)}(1/2)} \left[\ln \frac{T}{T_{c0}} + \psi' \left(\frac{1}{2} \right) \frac{eBD}{2\pi cT} \right]. \quad (22)$$

Inserting this expression into the BKT condition and taking a derivative with respect to the temperature yields

$$\left| \frac{dB_{c2}(T)}{dT} \right|_{T=T_c} = \frac{2\pi \hbar c}{eD \psi'(1/2)}. \quad (23)$$

The critical magnetic field at zero temperature, in contrast, is determined by the mean field condition $\alpha = 0$

$$B_{c2}(T = 0) = \frac{2\pi \hbar c}{eD} T_{c0} e^{\psi(1/2)}. \quad (24)$$

Using the expressions in Eqs. (23) and (24), we can write Eq (20) as

$$\frac{b(0) - b(t)}{t} = \left[1 + \sqrt{1 + \frac{C_1^2 d^2}{\epsilon a_0^2}} \right] \frac{\pi \chi T_{c0}}{24 \rho_{s0} d} \psi' \left(\frac{1}{2} \right) e^{\psi(1/2)}. \quad (25)$$

The final step in estimating $b(t)$ is to find the ratio of ρ_{s0} to the mean-field transition temperature T_{c0} . For moderately disordered superconductors, in the absence of any pair-breaking mechanism, semiclassical theory yields^{12,13}

$$\rho_{s0} = \pi \Delta \hbar \sigma_n / 4e^2 = 1.76 \pi \hbar \sigma_n T_{c0} / 4e^2. \quad (26)$$

We emphasize that the ratio ρ_{s0}/T_{c0} is expected to be reduced for strongly disordered superconductors^{14–16} with respect to the semiclassical formula in Eq. 26.

For ultra-thin films with $d \ll a_0$ we find, using Eqs. (25) and (26),

$$\frac{b(0) - b(t)}{t} = 0.8 \frac{e^2}{\hbar \sigma_n d} = 0.4 \pi \frac{R_{\square}}{R_Q} \equiv K \frac{R_{\square}}{R_Q}. \quad (27)$$

Here $R_Q = h/4e^2$ is the quantum of resistance for electron pairs and we used $\chi = 2/\pi$, as appropriate for the two-dimensional limit. Since this result relies on Eq. 26 that overestimates the ratio ρ_{s0}/T_{c0} , we expect to experimentally observe larger values for K . For thick films with $d \gg a_0$, Eqs. (25) and (26) imply that $|db/dt|$ grows linearly with R_{\square}/R_Q , i.e.,

$$\frac{b(0) - b(t)}{t} = \tilde{g}_0 \sqrt{\frac{e^2}{\hbar \sigma_n a_0}} + \tilde{K} \frac{R_{\square}}{R_Q}, \quad (28)$$

where $\tilde{g}_0 \approx 0.05\sqrt{C}$, and $\tilde{K} \approx 0.1$. Note that $|db/dt|$ does not extrapolate to zero as $R_{\square} = 1/\sigma_n d \rightarrow 0$. Similar to the result in the thin-film limit, the true numerical values of both \tilde{g}_0 and \tilde{K} are expected to be larger due to the lower value of ρ_{s0}/T_{c0} . Moreover, as explained in the main text, the coefficients \tilde{g}_0 and \tilde{K} can deviate from the values given by straightforward expansion of Eq. (25) for large d/a_0 . Such a deviation would reflect higher-order corrections to $\rho_s(T, B)$, which may become important in thick films.

¹ H. Kim, A. Ghimire, S. Jamali, T.K. Djidjou, J.M. Gerton, and A. Rogachev, Effect of magnetic Gd impurities on the superconducting state of amorphous Mo-Ge thin films with different thickness and morphology, *Phys. Rev. B* **86**, 024518

- (2012).
- ² P. W. Anderson, P. W., Theory of Flux Creep in Hard Superconductors, *Phys. Rev. Lett.* **9**, 309 (1962).
 - ³ Gurevich, A. V. and Mints, R. G., Self-heating in normal metals and superconductors, *Rev. Mod. Phys.* **59**, 941–999 (1987).
 - ⁴ Ovadia, M. and Sacépé, B. and Shahar, D. Electron-Phonon Decoupling in Disordered Insulators. *Phys. Rev. Lett.* **102**, 176802 (2009).
 - ⁵ Altshuler, B. L. and Kravtsov, V. E. and Lerner, I. V. and Aleiner, I. L. Jumps in Current-Voltage Characteristics in Disordered Films. *Phys. Rev. Lett.* **102**, 176803 (2009).
 - ⁶ Strnad, A. R. and Hempstead, C. F. and Kim, Y. B. Dissipative Mechanism in Type-II Superconductors. *Phys. Rev. Lett.* **13**, 794–797 (1964).
 - ⁷ Kim, Y. B. and Hempstead, C. F. and Strnad, A. R. Flux-Flow Resistance in Type-II Superconductors. *Phys. Rev.* **139**, A1163–A1172 (1965).
 - ⁸ Berghuis, P. and Kes, P. H. Two-dimensional collective pinning and vortex-lattice melting in a-Nb_{1-x}Ge_x films *Phys. Rev. B* **47**, 262–272 (1993).
 - ⁹ Xiao, Z. L. and Andrei, E. Y. and Paltiel, Y. and Zeldov, E. and Shuk, P. and Greenblatt, M. Edge and bulk transport in the mixed state of a type-II superconductor. *Phys. Rev. B* **65**, 094511 (2002).
 - ¹⁰ Thomann, A. U. and Geshkenbein, V. B. and Blatter, G. Dynamical Aspects of Strong Pinning of Magnetic Vortices in Type-II Superconductors. *Phys. Rev. Lett.* **108**, 217001 (2012).
 - ¹¹ Buchacek, M. and Willa, R. and Geshkenbein, V. B. and Blatter, G. Thermal depinning and creep in strong pinning theory. *arxiv:1802.00652*.
 - ¹² Abrikosov, A. A. and Gor'kov, L. P. Contribution to the theory of superconducting alloys with paramagnetic impurities. *Zh. Eksp. Teor. Fiz.* **39**, 1781 (1960) [*Sov. Phys. JETP* **12**, 1243 (1961)].
 - ¹³ M. Tinkham, *Introduction to Superconductivity*, Dover, 1996.
 - ¹⁴ Misra, S. and Urban, L. and Kim, M. and Sambandamurthy, G. and Yazdani, A. Measurements of the Magnetic-Field-Tuned Conductivity of Disordered Two-Dimensional Mo₄₃Ge₅₇ and InO_x Superconducting Films: Evidence for a Universal Minimum Superfluid Response *Phys. Rev. Lett.* **110**, 037002 (2013).
 - ¹⁵ Feigel'man, M. V. and Ioffe, L. B. and Kravtsov V. E. and Cuevas, E. Fractal superconductivity near localization threshold. *Ann. Phys.* **325**, 1390–1478 (2010).
 - ¹⁶ Feigel'man, M. V. and Ioffe, L. B. Superfluid density of a pseudogapped superconductor near the superconductor-insulator transition. *Phys. Rev. B* **92**, 100509 (2015).